Performance of Yokeless Heteropolar Electrodynamic Bearings

C. Dumont, V. Kluyskens, and B. Dehez

Department of Mechatronic, Electrical Energy, and Dynamic Systems (MEED)
Université catholique de Louvain, Louvain-la-Neuve, 1348, Belgium
corentin.dumont@uclouvain.be, virginie.kluyskens@uclouvain.be, bruno.dehez@uclouvain.be

Abstract ─ Electrodynamic bearings (EDBs) are a promising way to support rotors passively with no friction. In particular, heteropolar EDBs could allow for combining the motor and guiding functions, thereby optimizing the use of permanent magnets. Despite this advantage, few efforts have been dedicated to the evaluation and optimization of the performance of heteropolar EDBs. In this paper, the performance of a yokeless topology of heteropolar EDB is evaluated and optimized. This is done by evaluating the parameters of a parametric dynamical model of the EDB using a two-dimensional analytical model of the field distribution in the bearing. Compared to existing EDBs, the present one is shown to achieve a reasonable stiffness to permanent magnet volume ratio at high speeds.

Index Terms ─ Bearing, electrodynamic, heteropolar, magnetic, optimization, passive, performance.

I. INTRODUCTION

Passive electrodynamic bearings (EDBs) allow to support a rotating object without contact. They are based on the electromagnetic interaction forces between permanent magnets (PMs) and the currents flowing in conductors. These currents are induced by the relative speed between the PMs and the conductors.

For efficiency purposes, EDBs are designed in such a way that there is no variation in the PM flux linked by the winding when the rotor spins in a centered position. As a result, there are no induced currents, no forces, and above all no losses in the bearing when the rotor spins in a centered position. This property is referred to as "null-flux". It is found in all the designs of EDBs that are studied nowadays [1].

However, when the rotor spins in an off-centered position, currents are induced in the winding. This creates a force on the rotor that tends to restore its centered position. In this case, the energy dissipated in the windings comes from the drive torque on the rotor to keep the spin speed constant. On the one hand, this prevents the operation at zero spin speed. On the other hand, it eliminates the need for an additional electrical power supply to feed the EDBs, as is the case for the

existing active magnetic bearings (AMBs). Furthermore, the absence of control system induces gains in compactness, simplicity, costs and reliability. As a result, EDBs could be well suited for applications where these aspects are critical.

Nevertheless, the stiffness associated with the centering force of EDBs is low compared with AMBs. Moreover, some external damping must be added to the system to allow a stable operation above a given spin speed [2]. In this paper, only non-rotational damping between the rotor and the stator is considered. This damping should be added in a passive way in order to keep the advantages of passive bearings, which can be an issue [2]. Consequently, the bearing radial stiffness and the amount of damping required for stabilization are the main quality indices of an EDB.

For the last 15 years, the research on EDBs has focused on homopolar topologies, which constitute most of the implementations of EDBs nowadays [3-5]. This resulted in significant progress in their modeling, allowing for accurate predictions of their behavior and performance.

As opposed to their heteropolar counterparts, homopolar EDBs can be built using bulk conductors [3] [5], resulting in simple and robust bearing designs. They also allow for filtering the force excitations that are synchronous with the spin speed [6]. Therefore, in case of rotor unbalance, the rotor can spin around its axis of inertia without transmitting forces to the housing. However, the homopolar field source could hardly be coupled to a winding to create a torque, which is the case in heteropolar EDBs. Despite this advantage, the actual potential of heteropolar EDBs still needs to be evaluated.

In this context, the paper presents an optimization of the performance of the heteropolar EDB introduced in [7]. Although the chosen bearing topology can perform the motor function, the present optimization concerns only the guiding function in the aim of providing an upper limit for the performance of this kind of bearing.

The paper is organized as follows. In Section II, the bearing topology and model are presented, as well as the model parameters identification process. In Section III, the EDB optimization is described and the results are

analyzed. Finally, the performance of the optimal bearings are compared to the performance of existing homopolar EDBs in Section IV.

II. MODELING AND PERFORMANCE EVALUATION

The EDB topology studied in this paper is shown in Fig. 1.
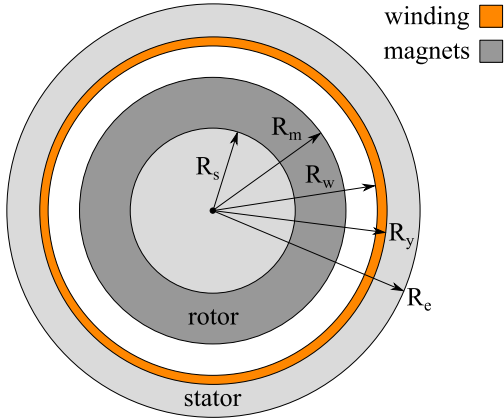
Fig. 1. Bearing topology and design parameters.

The rotor PMs have one pole pair. The winding has three phases (Fig. 2) and two pole pairs in order to have the null-flux characteristic [8].
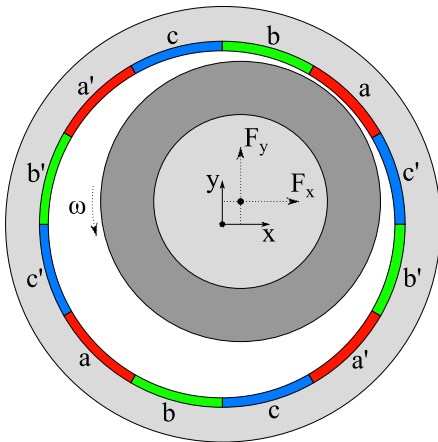
Fig. 2. Rotor position, electrodynamic forces and winding phases.

The properties of the bearing materials are given in Table 1. As regards the modeling assumptions, the magnetic permeability of the shaft iron is infinite and the materials have linear magnetic characteristics, i.e., magnetic hysteresis and saturation are neglected. The eddy currents in bulk materials and the impact of the rotor off-centering on the winding inductances are also neglected.

Table 1: Bearing material properties

Parameters	Units	Definition
$\rho_m = 7500$	kg/m^3	Specific mass of the NdFeB magnets
$B_r = 1.2$	T	PM remanent magnetization
$\rho_s = 7800$	kg/m^3	Specific mass of the shaft iron
$\sigma_{cu} = 6e7$	$(\Omega m)^{-1}$	Copper conductivity
$\mu_s = \infty$	/	Relative magnetic permeability of the shaft iron
$\mu_r = 1$	/	Relative magnetic permeability of the winding, magnets, and stator yoke

The dynamics of the rotor is studied using the Jeffcott rotor model. Therefore, the rotor is assumed to move in the radial plane only. Using complex coordinates, the position of the rotor and the electrodynamic forces are:

$$z = x + jy, \quad (1)$$
$$F = F_x + jF_y. \quad (2)$$

They are linked with the external input force $\boldsymbol{F_e}$ through the state-space model [9]:

$$\begin{bmatrix} \dot{F} \\ \ddot{z} \\ \dot{z} \end{bmatrix} = A \begin{bmatrix} F \\ \dot{z} \\ z \end{bmatrix} + BF_e, \quad (3)$$

where the dynamic and input gain matrices are:

$$A = \begin{bmatrix} -\dfrac{R}{L_c} - j\omega & -\dfrac{3K_\Phi^2}{2L_c} & -j\omega\dfrac{3K_\Phi^2}{2L_c} \\ \dfrac{1}{M} & -\dfrac{C}{M} & 0 \\ 0 & 1 & 0 \end{bmatrix}, \quad (4)$$

$$B = \frac{1}{M}[0 \quad 1 \quad 0]^T. \quad (5)$$

The parameters in (4)-(5) are given in Table 2. As the bearing is studied in 2D, all the parameters and performance indices are evaluated per unit of active bearing length. The parameters $\boldsymbol{R}$, $\boldsymbol{L_c}$, and $\boldsymbol{K_\Phi}$ are identified using the 2D analytical model presented in [7] with the material properties listed in Table 1. In particular, $\boldsymbol{K_\Phi}$ is the ratio of the peak PM magnetic flux in a winding phase to the amplitude of the rotor off-centering $|\boldsymbol{z}|$. The rotor is assumed to weigh three times the weight of its active length, which yields:

$$M = 3[\rho_m\pi(R_m^2 - R_s^2) + \rho_s\pi R_s^2], \quad (6)$$

where ρ_m and ρ_s are given in Table 1. Lastly, the spin speed ω and the damping C are set arbitrarily.

Table 2: Parameters of the dynamical model

Parameters	Units	Definition
R	Ω/m	Winding phase resistance
L_c	H/m	Winding cyclic inductance
M	kg/m	Rotor mass
K_Φ	$\left(\dfrac{N\Omega s}{m^3}\right)^{0.5}$	Flux constant
C	Ns/m^2	External non rotating damping
ω	rad/s	Rotor spin speed

From these parameters, the two bearing performance indices can be calculated. The bearing quasi-static radial stiffness is derived from (3):

$$K = \Re e \left\{ \frac{F}{z} \right\} \bigg|_{\dot{z}=0,\ddot{z}=0,\dot{F}=0} = \frac{3\omega^2 L_c K_\Phi^2}{2(R^2 + (\omega L_c)^2)}. \quad (7)$$

Lastly, the damping required for stabilization C_s is obtained by increasing the value of C until the three eigenvalues of (4) cross the imaginary axis.

III. OPTIMIZATION

The bearing is optimized using a NSGA-II genetic algorithm with 100 individuals and 100 iterations. The mutation probability is 0.3, and the crossover rate is 0.9. From this, a Pareto front of optimal solutions that defines the area of achievable performance is obtained. The two objective functions K and C_s are optimized at a given spin speed ω rad/s. Defining the variables of the optimization problem:

$$x_1, x_2 \in [0,1], \quad (8)$$

the constraints on the geometric parameters can be formulated as:

$$R_m = x_1 R_{m,max}, \quad (9)$$
$$R_s = 0.2 R_m, \quad (10)$$
$$R_w = R_m + 1.5mm, \quad (11)$$
$$R_y = R_w + x_2 (\beta R_{m,max}). \quad (12)$$

In (9)-(12), the arbitrary parameters are set in order to get the best possible results, and thus an upper bound for the bearing performance. In (9), the maximum rotor radius $R_{m,max}$ is constrained by the maximum rotor peripheral speed $v_{max} = 250$ m/s:

$$R_{m,max} = \max(R_m) = \frac{v_{max}}{2\pi\omega}. \quad (13)$$

This is a realistic value for PM rotors with a retaining sleeve [10, 11]. In (10), the ratio of the rotor shaft radius to magnet radius is 0.2. This low value yields better results as the amount of magnet, and thus the bearing performance are maximized. In (11), the air gap width is set at 1.5 mm, which includes the width of a potential sleeve and allows for rotor eccentricities. In (12), the maximum winding thickness is related to the maximum rotor thickness $R_{m,max}$ through the factor $\beta = 1$. This allows the algorithm to explore a large yet realistic range of winding thicknesses.

Let us analyze the results for $\omega = 2\pi 1000$ rad/s and $\beta = 1$. The Pareto front in Fig. 3 shows that the damping required for stabilization increases with the bearing stiffness. The graph was limited to values of $C_s < 500$ Ns/m², which can be considered as very large for damping added in a passive, contactless way. Damping values of an order of magnitude of 10 Ns/m are reported in the literature [4].

Regarding thermal limitations, the winding current densities for each individual on the Pareto front are presented in Fig. 4. The losses are calculated assuming a static eccentricity of the rotor with an off-centering

$z = 0.5(R_w - R_m)$. In this case, the current density always lies below the maximum value of 5 A/mm² that is typical of enclosed PM machines [12]. In Fig. 4, the individuals are arranged in the same order as in Fig. 3, the individuals with lower stiffnesses on the left-hand side and the individuals with higher stiffnesses on the right hand side. This will be the case for all the figures in the following sections.
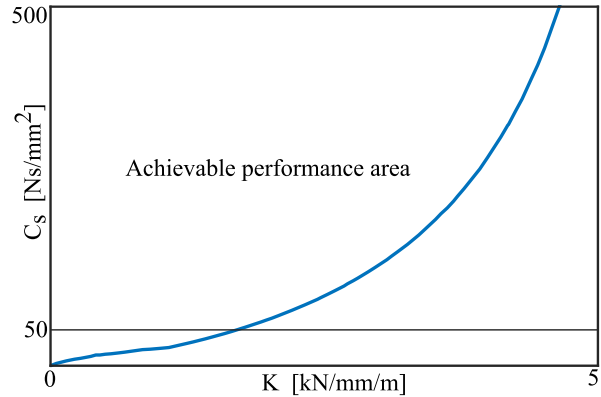
Fig. 3. Pareto front of the bearing performance at $\omega = 2\pi 1000$ rad/s.
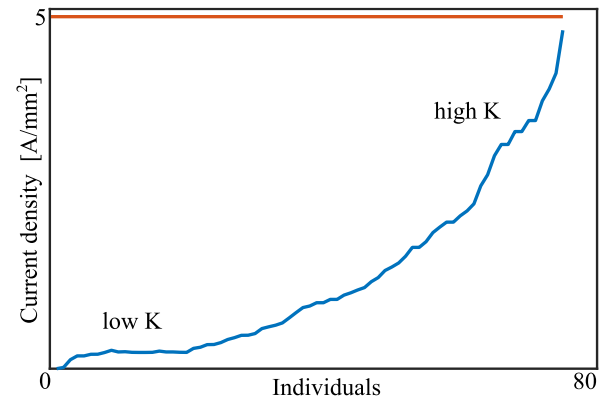
Fig. 4. Current densities associated with the individuals on the Pareto front, and maximum value of 5 A/mm².

Figures 5 and 6 show that bearings with a thicker winding require less damping for stabilization. This is the case for the individuals 1-20 with winding thicknesses nearing the maximum value. It corresponds to expectations as a lower winding resistance yields a more inductive behavior of the bearing that is known to have a positive effect on the stability [4, 7].

On the contrary, the individuals 20-80 have a greater PM thickness and the winding is closer to the PM on average. As a result, the magnetic field strength and the bearing stiffness are higher. However, the winding is more resistive as $(R_y - R_w)$ decreases, which affects the stability.
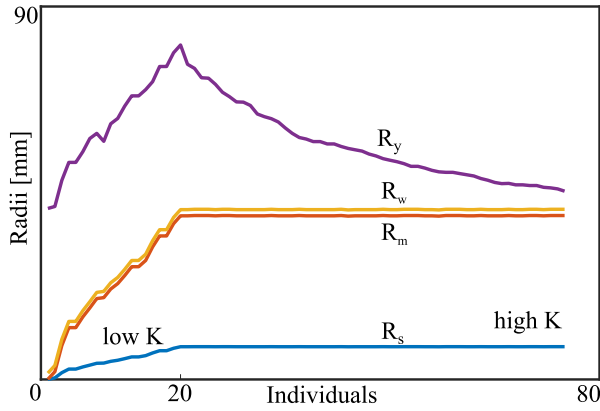
Fig. 5. Geometrical parameters of the individuals on the Pareto front for $\omega = 2\pi 1000$ rad/s.
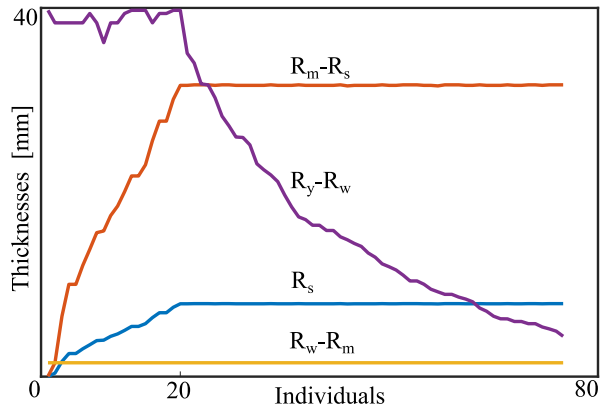
Fig. 6. Width of the shaft (R_s), PMs ($R_m - R_s$), air gap ($R_w - R_m$) and winding ($R_y - R_w$).

The Pareto fronts corresponding to the spin speeds $\omega = 2\pi\{50,100,500,1000\}$ rad/s are shown in Fig. 7. For a given value of K, more damping is required to stabilize the bearings running at higher speeds. This is due to the mechanical constraint on the peripheral speed. The value of $R_{m,max}$ is lower for the individuals running at higher speeds, which lowers the volume of PMs. An absence of the constraint on the peripheral speed would yield opposite results, as a given winding is more inductive while running at higher speeds.

Finally, the graphs of the bearing geometrical parameters in the cases $\omega = 2\pi\{50,100,500\}$ rad/s have a shape similar to that of the $\omega = 2\pi 1000$ rad/s case. In each case, the crosses in Fig. 7 and in the zoomed view in Fig. 8 indicate the individuals that have PMs and winding widths close to their maximum values. For instance, it is the 20th individual in the case of $\omega = 2\pi 1000$ rad/s (Fig. 6). For individuals lying further to the left on the Pareto front, the winding thickness reaches its maximum value, whatever the spin speed. In this area,

the Pareto fronts for all the speeds are almost superimposed, as shown in Fig. 8 ($\beta = 1$). Furthermore, the values of damping lie in the range $C_s \in [0,50]$ Ns/m in this figure, which is more realistic. As a result, a bearing optimized under the constraints (9)-(13) requires a same amount of damping for a given stiffness, whatever the spin speed.
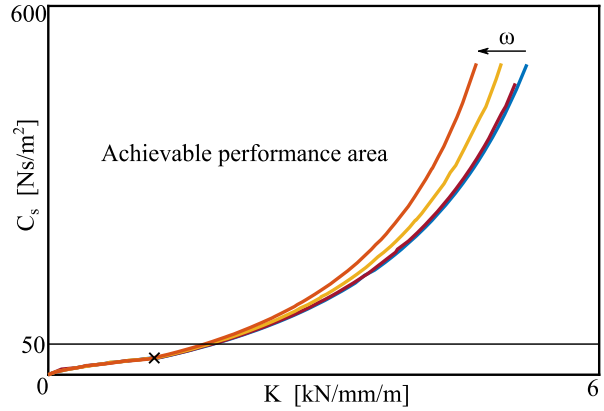
Fig. 7. Pareto fronts for $\omega = 2\pi\{50, 100, 500, 1000\}$ rad/s.
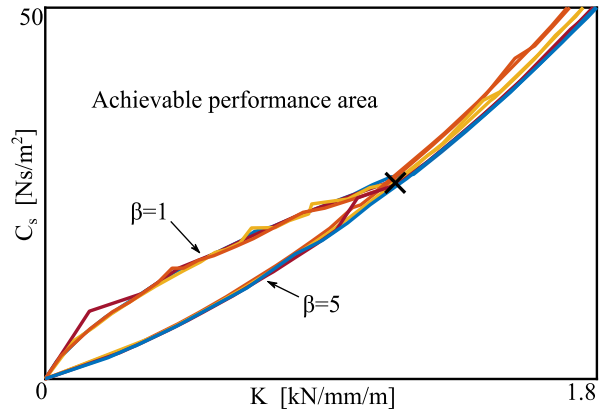
Fig. 8. Zoom on the area of interest where $C_s < 50$ Ns/m.

For $\omega = 2\pi\{50,100,500\}$ rad/s, the winding current densities lie far below the limit of 5 A/mm^2.

Lastly, Fig. 8 shows the Pareto fronts corresponding to $\beta = 5$ in (12). As expected, the corresponding area of achievable performance is larger, because increasing β allows the algorithm to explore a wider range of winding thicknesses, although they may be unrealistic. These fronts constitute an absolute performance limit, as further increasing β has no impact on their positions.

Finally yet importantly, the Pareto fronts in Figs. 7-8 constitute an upper performance bound as considering additional constraints and/or the end-effects may reduce the performance of the bearing under study.

IV. PERFORMANCE COMPARISON

The performance of existing EDBs were summarized in [1]. The stiffness to PM volume ratios were calculated, yielding the black triangles in Fig. 9. The ranges given by the vertical bars correspond to the EDBs lying on the Pareto front in Fig. 7.
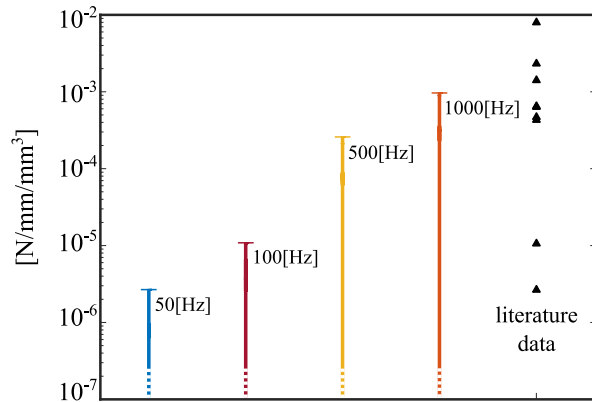
Fig. 9. Stiffness to volume ratio of the existing EDBs (triangles) and of the individuals on the Pareto fronts of Fig. 7 (solid lines).

The overall shape of the graph shows that bearings operating at higher spin speeds can achieve higher ratios. Compared with existing EDBs, the present topology provides a reasonable ratio at high speed, although it was not optimized considering this specific criterion.

V. CONCLUSION

In this paper, the domain of achievable performance of a heteropolar EDB was obtained by generating a Pareto front using an optimization algorithm. The two performance indices, namely the stiffness and the damping required for stabilization, were evaluated by combining two analytical models predicting the field distribution in the EDB and its dynamic behavior. The domain of achievable performance was obtained for different spin speeds. This highlighted a clear trade-off between stiffness and stability.

Then, the bearings lying on the Pareto front were compared to existing EDBs in terms of stiffness to volume ratio. It was shown that ratios similar to that of existing EDBs can be achieved at high speeds with the present EDB topology. This ratio could be further optimized as it was not an objective function of the present optimization.

Future work should include a study of both motor and bearing functions to take their respective constraints into account, and more especially thermal constraints.

REFERENCES

[1]   J. G. Detoni, "Progress on electrodynamic passive magnetic bearings for rotor levitation," *Proc. Inst.,*
Mech., Eng., Part C: J. Mech. Eng. Sci., vol. 228, pp. 1829-1844, 2014.

[2]   A. Tonoli, N. Amati, F. Impinna, and J. G. Detoni, "A solution for the stabilization of electrodynamic bearings: Modeling and experimental validation," *J. Vib. Acoust.*, vol. 133, no. 2, 2011.

[3]   T. A. Lembke, "Design and analysis of a novel low loss homopolar electrodynamic bearing," *Ph.D. Dissertation*, Royal Inst. Tech., Sweden, 2005.

[4]   A. V. Filatov and E. H. Maslen, "Passive magnetic bearing for flywheel energy storage systems," *IEEE Trans. Magn.*, vol. 37, no. 6, pp. 3913-3924, 2001.

[5]   J. G. Detoni, "Developments on electrodynamic levitation of rotors," *Ph.D. Dissertation*, Politecnico di Torino, Turin, Italy, 2012.

[6]   J. G. Detoni, F. Impinna, A. Tonoli, and N. Amati, "Unified modelling of passive homopolar and heteropolar electrodynamic bearings," *J. Sound and Vibrations*, vol. 331, no. 19, pp. 4219-4234, 2012.

[7]   C. Dumont, V. Kluyskens, and B. Dehez, "Yokeless radial electrodynamic bearing," *Mathematics and Computers in Simulation*, vol. 130, pp. 57-69, 2016.

[8]   C. Dumont, V. Kluyskens, and B. Dehez, "Null-flux radial electrodynamic bearings," *IEEE Trans. Magn.*, vol. 50, no. 10, pp. 1-12, 2014.

[9]   C. Dumont, V. Kluyskens, and B. Dehez, "Linear state-space representation of heteropolar electro-dynamic bearings with radial magnetic field," *IEEE Trans. Magn.*, vol. 52, no. 1, pp. 1-9, 2016.

[10] A. Binder and T. Schneider, "High-speed inverter-fed AC drives," *2007 International Aegean Conference on Electrical Machines and Power Electronics*, Bodrum, pp. 9-16, 2007.

[11] A. Borisavljevic, *Limits, Modeling and Design of High-Speed Permanent Magnet Machines*, Springer-Verlag Berlin Herdelberg, 2013.

[12] D. G. Dorrell, M.-F. Hsieh, M. Popescu, L. Evans, D. A. Staton, and V. Grout, "A review of the design issues and techniques for radial-flux brushless surface and internal rare-earth permanent-magnet motors," *IEEE Trans. Magn.*, vol. 58, no. 8, pp. 3741-3757.

Corentin Dumont was born in Belgium in 1989. He received the Electromechanical Engineering degree in 2012 and the Ph.D. degree in 2017 from the Université catholique de Louvain (UCL), Belgium. He is currently a Researcher at the Department of Mechatronic, Elect-

rical Energy, and Dynamic Systems (MEED) of the Université catholique de Louvain (UCL). His research focuses on magnetic bearings.

Virginie Kluyskens was born in Belgium, in 1980. She received the Electromechanical Engineering degree in 2004 and the Ph.D. degree in 2011 from the Université catholique de Louvain (UCL), Louvain-la-Neuve, Belgium. She is currently Senior Researcher at the MEED Department of the UCL. Her research interests are in the field of passive magnetic bearings.

Bruno Dehez was born in Belgium, in 1975. He received the degree in Electromechanical Engineering and the Ph.D. degree from the Université catholique de Louvain (UCL), Louvain-la-Neuve, Belgium, in 1998 and in 2004, respectively. He is currently a Professor at the Ecole Polytechnique de Louvain (EPL), and is Head of the MEED Department of the UCL. His research interests are in the field of design and optimization of electro-magnetic devices, and particularly of electrical machines and actuators.